

# Origin of granular axial segregation bands in a rotating tumbler: an interface-mixing driven Rayleigh-Taylor instability

Umberto D’Ortona\*

*Aix-Marseille Université, CNRS, Centrale Marseille, M2P2, Marseille, France*

Richard M. Lueptow

*Department of Mechanical Engineering, Northwestern University, Evanston, Illinois 60208, USA and*

*Department of Chemical and Biological Engineering,  
Northwestern University, Evanston, Illinois 60208, USA*

Nathalie Thomas

*Aix-Marseille Université, CNRS, IUSTI, Marseille, France*

(Dated: October 16, 2024)

The origin of large and small particle axial bands in long rotating tumblers is a long-standing question. Using DEM simulations, we show that this axial segregation is due to a Rayleigh-Taylor instability which is characterized by the fact that the density of a granular medium increases with mixing and decreases with segregation. For initially mixed particles, segregation and collisional diffusion in the flowing layer balance and lead to a three-layer system, with a layer of large particles over a layer of small particles, and, interposed between these layers, a layer of more densely packed mixed particles. The higher density mixed particle layer over the lower density small particle layer induces a Rayleigh-Taylor instability, evident as waviness in the interface between the layers. The waviness destabilizes into ascending plumes of small particles and descending plumes of mixed particles with large particles enriched near the surface, which become evident as small and large particle bands visible at the free surface. Rolls driven by segregation at the tilted interface between plumes maintain the pattern of frozen plumes.

Introduction—Rayleigh-Taylor (RT) instabilities arise when a denser fluid is placed atop a lighter one in a gravitational field, and the horizontal interface between the layers becomes wavy [1, 2]. The amplitude of the waviness increases, eventually resulting in downward high density plumes and upward low density plumes. In its simplest form, the density difference originates from the use of distinct fluids, either miscible or immiscible. However, RT instabilities are also observed in more complex situations including chemical reactions at an interface forming a third layer with a density difference [3–5], the dissolution of a gas in a liquid [6], and the accumulation of particles [7, 8] or bubbles [9] at the interface of two liquids. In these last examples, a third layer, denser or lighter, can appear in between the two initial layers creating a 3-layer RT instability, which has been addressed theoretically [10–12]. A special situation of interest for this study occurs in some of these systems (autocatalytic reaction front [4], granular rafts [8], CO<sub>2</sub> chemisorption [6], or simply a single thin layer of liquid bounded by an upper wall [13]), where the RT instability initiates the interfacial waviness and then ascending or descending plumes start to form. But for different reasons, the plumes do not evolve further, so that a frozen pattern of protrusions results instead of the ongoing plumes that usually cause the eventual total reversal of the dense and light layers following the RT instability.

Rayleigh-Taylor instabilities can also occur in granular flows. Unlike the fluid instability, the granular layers must be flowing for the instability to occur (static granular layers would remain unchanged without the input of energy via the flow). For example, for flow down a rough inclined chute with a layer of large dense particles above a layer of small light particles, the interface between the layers destabilizes to form ascending plumes of the small light particles and descending plumes of large dense particles in a spanwise-depthwise cross-section of the flow [14]. These plumes appear at the surface as parallel stripes of the two particle species extending in the streamwise direction, and they can be sustained by counter-rotating Rayleigh-Bénard-like convection rolls between the plumes where the convection rolls are driven by granular size segregation. This granular RT instability can even occur with initially mixed particles flowing down an incline: large dense particles initially segregate upward so that they accumulate in a dense particle layer that destabilizes to the plume pattern. Because the unstable state forms spontaneously as the granular material is flowing, it has been termed self-induced RT instability [14]. The objective of this letter is to explain how a granular Rayleigh-Taylor instability causes the axial segregation of particles having two sizes, even though the particles have the same density, which may seem paradoxical.

Axial segregation occurs in long horizontal cylindrical rotating tumblers that are partially filled with a mixture of small and large particles. Upon rotation, particles tumble down the inclined surface in a thin flowing layer,

---

\* umberto.dortona@cnrs.fr

while particles below this flowing layer are in a static zone that is in solid body rotation with the tumbler. It is well-known that within a few tumbler rotations, radial size segregation occurs in which small particles percolate to the bottom of the surface flowing layer forcing large particles to rise to the top of the flowing layer [15–17]. Thus, there is a layer of large particles over a layer of small particles flowing down the inclined free surface of the granular bed, while the particles below the flowing surface layer are in solid body rotation. After many more tumbler rotations following radial segregation, axially spaced bands rich in small or large particles appear (Fig. 1) [18–21]. Although first reported in 1940 [22], axial segregation did not attract attention until much later [15, 19–21, 23–28], and it remains unexplained. The axial bands typically have a wavelength of approximately one tumbler diameter [29–32], although they eventually tend to merge and coarsen [20, 30–36]. The bands can occur, or not occur, under a wide range of conditions including various fill levels, rotation speeds, particle shape and size, species concentrations, tumbler cross-sections, with submerged as well as dry particles, and in tilted tumblers [31, 36–38]. When observed using an index-matched interstitial fluid or magnetic resonance imaging, small particle bands correspond to regions where the radially-segregated core of small particles extends to the flowing layer surface; large particle bands comprise an annulus of large particles surrounding the core of small particles [26, 37–42], evident at the right end of the domain in Fig. 1.

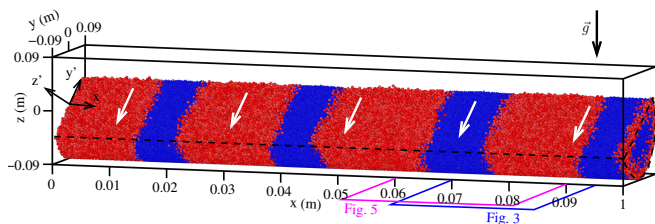


FIG. 1. DEM simulation of axial segregation bands in a 100 cm long, 18 cm diameter tumbler rotating at 15 rpm that is half filled with equal volume fractions of 2 mm (blue) and 5 mm (red) spherical particles with periodic boundary conditions at 1400 s (350 rotations), when the bands are stationary.

Proposed mechanisms for axial bands include differences in the angle of repose [19, 25, 26] or mobility of particle species [25, 28], and the concept of ‘negative diffusivity’ has been used to rationalize axial segregation [19, 26, 43, 44]. However, these concepts address how bands might be reinforced, not their origin [21, 39, 42] nor the subsurface bulges in the radially segregated core of small particles that precede visible bands at the surface [21, 35, 45]. What is known is that bands of large particles typically first appear near the tumbler endwalls [15, 18, 19, 36, 38, 42, 46, 47] due to the interaction between endwall friction and radial segregation [15, 42, 48–51]. However, the initial band formation at the endwalls does not explain bands that initiate near the middle of

a tumbler [42] or bands that form with periodic endwall conditions (Fig. 1) [42].

Here, we propose a mechanism for axial segregation and band formation that is related to the recent discovery of a granular flow instability [14] that is analogous to the fluid RT instability occurring when a static dense fluid is atop a static less dense fluid. A hint that the granular RT instability may be connected to axial band formation in rotating tumblers is that bands form more readily for mixtures when the large particles are slightly more dense than small particles [21, 52]. Indeed, we demonstrate here that a granular RT instability induces band formation of size-bidisperse iso-density particles in rotating tumblers, and the segregated axial bands of particles are maintained by the emergence of streamwise counter-rotating rolls driven by size segregation. The excess density necessary for a RT instability is a consequence of a property of granular materials: a polydisperse granular mixture can pack more densely than monodisperse particles and, hence, has a greater bulk density [53, 54]. A RT instability resulting from the bulk higher density of mixed polydisperse particles has, to our knowledge, never been reported for granular flows.

**Simulations**—The Discrete Element Method (DEM) code LIGGGHTS [55, 56] is used to explore size-bidisperse granular flow in a smooth frictional tumbler wall having inner diameter  $D = 2R = 18$  cm and length  $L = 100$  cm, using periodic boundary conditions at the ends of the computational domain to avoid any frictional effects that would occur if frictional endwalls were used. Tumblers are half-filled with equal volumes of small (diameter  $d = 2$  mm) and large particles (various diameters  $d_l > 2$  mm). Particle properties correspond to cellulose acetate: density  $\rho = 1308$  kg m<sup>-3</sup>, restitution coefficient  $e = 0.87$  [57–59], friction coefficient  $\mu = 0.7$ , and uniform size distributions of 0.95–1.05 times  $d$  or  $d_l$ . Particle interactions are calculated using a linear contact model with Young’s modulus  $E = 10^7$  Pa and Poisson’s ratio  $\nu = 0.3$ . The integration time step is  $5 \times 10^{-6}$  s to provide stable results. Particles are initially randomly distributed within the tumbler volume at zero gravity. Then gravity ( $g = 9.81$  m s<sup>-2</sup>) and tumbler rotation are turned on simultaneously so that the mixed particles fall to the bottom of the tumbler and flow due to tumbler rotation at  $\omega = 15$  rpm (Froude number  $Fr = \omega^2 R/g = 0.023$ ) in a steady flowing layer at the free surface that is essentially flat above a static region that is in solid body rotation.

**Segregation time evolution**—To quantify the evolution of the degree of axial segregation, we compute  $I_{\text{seg}}(t) = (1/L) \int_0^L |\bar{f}_l - f_l(x,t)| + |\bar{f}_s - f_s(x,t)| dx$ , where  $f_i(x,t)$  is the volume fraction for species  $i$  averaged across the  $y-z$  plane in the particle bed at axial position  $x$  and time  $t$ , and the average species volume fraction in the tumbler is  $\bar{f}_s = \bar{f}_l = 0.5$ , where subscripts  $s$  and  $l$  refer to small and large particles, respectively.  $I_{\text{seg}} = 0$  corresponds to no axial segregation when the two particle species are completely mixed or when there is an axially-invariant radial core of small particles. Perfect axial segregation

with axial bands of pure small or pure large particles corresponds to  $I_{\text{seg}} = 1$ . Note that for most axial segregation experiments it is only the appearance of bands at the surface or through clear tumbler walls that is observed [31, 33, 34, 36], whereas  $I_{\text{seg}}$  measures segregation that can manifest as subsurface bulges in the radial segregation core [26, 27, 37–42]. The time evolution of  $I_{\text{seg}}$  indicates how quickly axial segregation occurs, and the value at which  $I_{\text{seg}}$  plateaus indicates the steady-state degree of axial segregation.

Although we consider a wide range of conditions in a companion paper, here we provide an example of how the particle size ratio,  $d_i/d$ , affects the evolution of the axial segregation,  $I_{\text{seg}}$ , for  $D/d = 90$  (Fig. 2). In all cases,  $I_{\text{seg}}$  evolves approximately exponentially at first, followed by linear growth before it flattens and reaches a plateau. The growth rate increases with  $d_i/d$ , consistent with previous experiments [21], and saturates for  $d_i/d \geq 2.5$ . The plateau for  $I_{\text{seg}}$  is highest for  $d_i/d = 2.25$  and 2.5 (the case we consider in detail), a consequence of the lower propensity for size segregation at smaller and larger  $d_i/d$  [60].

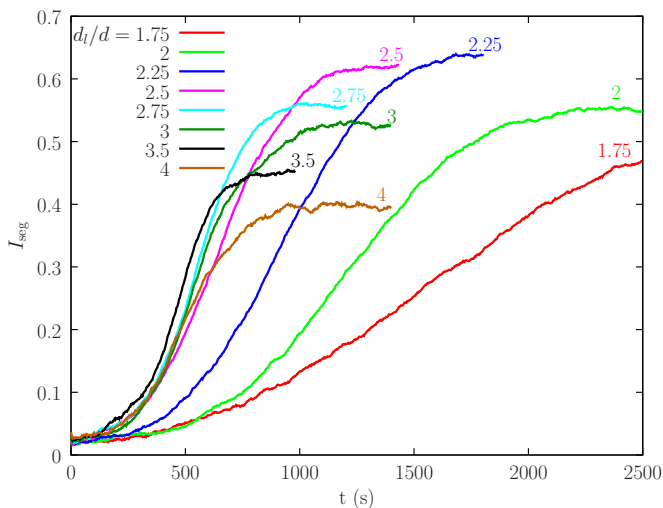


FIG. 2. Evolution of  $I_{\text{seg}}$  for  $1 < d_i/d \leq 4$  and  $L/d = 500$ .

**Band formation mechanisms**—We propose that after initial radial segregation of large and small particles, axial segregation comes about due to a granular RT instability in the flowing layer much like that for a two-layer flow of large dense particles above small light particles [14]. The axially segregated pattern is maintained by streamwise recirculation rolls that repeatedly redistribute the large and small particles mixed by diffusion at the interface into their own band.

The distributions of large and small particles ( $d_i/d = 2.5$ ) in the flowing layer and the overall particle volume fraction,  $\phi$ , are shown in Fig. 3 for radial segregation and subsequent formation of the bands. Radial segregation occurs quickly after the start of rotation with large particles (red) at the flowing layer surface and small particles (blue) segregated below them within  $t = 15$  s (3.75

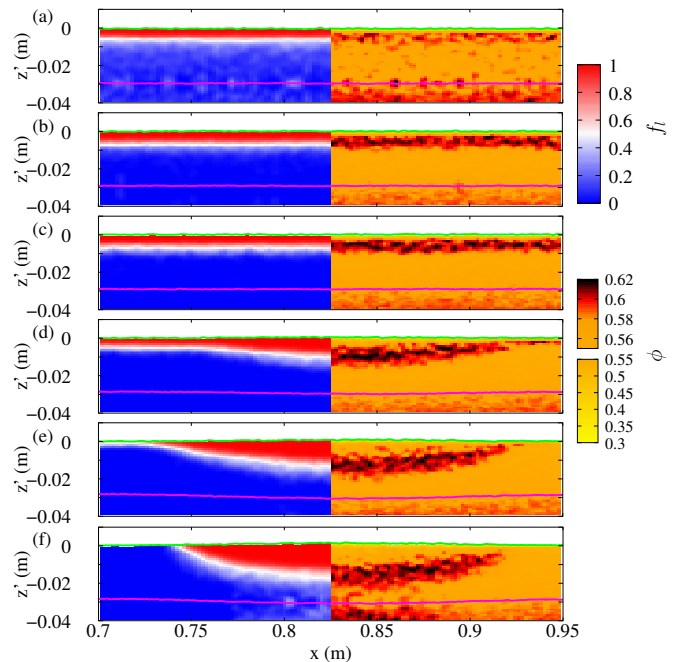


FIG. 3. Large particle species fraction,  $f_1$  (red-blue colorbar), and particle volume fraction,  $\phi$  (yellow-black colorbar), at (a)  $t = 15$  s, (b)  $t = 30$  s, (c)  $t = 50$  s, (d)  $t = 500$  s, (e)  $t = 700$  s and (f)  $t = 1250$  s in the  $x - z'$  plane at  $y' = 0$  ( $d_i/d = 2.5$ ). Only the flowing region ( $0 \lesssim z' \lesssim 0.04$  m) is shown. Green lines indicate the free surface ( $\phi = 0.3$ ), and magenta lines indicate the bottom of the flowing layer.

tumbler rotations, Fig. 3(a)), consistent with previous results [15–21]. As radial segregation progresses, which corresponds to segregation normal to the free surface in the  $z'$ -direction, the large and small particle layers become more concentrated ( $t = 30$  s, Fig. 3(b)), so that by  $t = 50$  s (12.5 tumbler rotations) the  $z'$ -direction segregation reaches a quasi-stationary state, in which the segregation between the two species is incomplete (Fig. 3(c)). The mixed particle interface (the white color corresponds to a 50:50 mixture) between the large and small particle layers results from a balance between size segregation and mixing. The balance between segregation and diffusive mixing allows the analytical solution of the vertical particle fraction profile for a steady state segregated bidisperse chute flow [61–63] or simple shear flow [64], and, thus, the thickness of the mixing zone. However, a similar analysis is difficult for tumbler flow because particles continually enter and exit the flowing layer as the tumbler rotates.

The right part of Fig. 3 presents the particle volume fraction  $\phi$ . As radial segregation progresses, a dense layer forms around  $z' \simeq -0.01$  m corresponding to the mixed particle region. At the quasi-stationary state (Fig. 3(c)), the particle volume fraction varies with depth from  $\phi \approx 0.55$  (orange) for pure large particles at the surface, to  $\phi \approx 0.62$  (black) for mixed particles (which pack more densely than monodisperse particles), and then to

$\phi \approx 0.55$  (orange) for pure small particles. The maximum of  $\phi \approx 0.62$  corresponds to  $f_l \approx 0.72$  (pink on the colorscale), evident as the small vertical shift between the black and white regions in Fig. 3(c).

We contend that for particles of the same density, the layer of mixed particles with  $\phi \approx 0.62$  above the layer of small particles with  $\phi \approx 0.55$  can provide a sufficient difference in the bulk densities for the granular RT instability to occur. Figure 3(c-f) shows the evolution of the RT instability beginning with a downward protrusion of mixed particles at  $t = 500$  s (d) and an upward protrusion of small particles that has broken the free surface by  $t = 700$  s (e), thereby forming stationary axially segregated bands at  $t = 1250$  s (f). Both the degree of segregation and the amplitude of a sinusoidal fit to the waviness of the mixed particle layer (white on the left side of Fig. 3) have been measured to grow exponentially until the small particles break the surface, as expected for a RT instability [1, 2]. This process is unusual compared to most RT instabilities in that it occurs for a high density layer linked to the mixture that is created by diffusion and loses its excess density by segregation. The resulting small particle band (blue) extends from the core to the free surface with the annular large particle band (red) surrounding the core, consistent with previous results [26, 37–39, 41, 42].

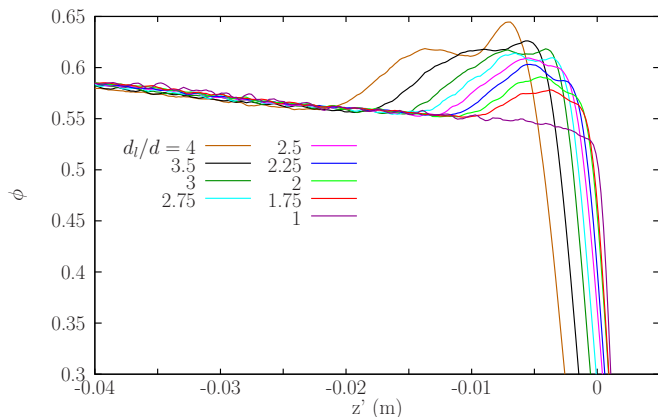


FIG. 4. Depthwise profile of the particle volume fraction  $\phi$  at  $y' = 0$  for  $1 \leq d_i/d \leq 4$  when axial band formation is suppressed by using a short 10 cm long tumbler ( $L/d = 50$ ).

Depthwise profiles of  $\phi$  after radial segregation is established but before bands form demonstrate how  $\phi$  for the mixed layer depends on  $d_i/d$ . Figure 4 presents smoothed profiles of  $\phi$  obtained using a tumbler too short for bands to form [29–32] allowing a long integration time ( $50 \leq t \leq 100$  s). Profiles of  $\phi$  are taken halfway down the flowing layer averaged over a 1 cm thick slice in the  $x - z'$  plane. The bottom of the flowing layer is at  $z' \approx -0.04$  m, and the free surface is at  $z' \approx 0$ , where  $\phi$  decreases sharply. For all size ratios, there is a region around  $z' = -0.005$  m where  $\phi$  is significantly larger, indicating a denser layer of mixed particles above a less dense layer of monodisperse small particles. The excess

in bulk density, typically around 10%, is what drives the RT instability, even without any density difference between the particle species.

Figure 4 shows that  $\phi$  in the mixed layer increases with increasing  $d_i/d$ , as would be expected for more efficient packing at higher  $d_i/d$ . For  $d_i/d = 1$  to 2.5, the maximal  $\phi$  near the surface increases with a bump that is relatively narrow, but for  $d_i/d = 2.5$  to 4, the maximum only increases slightly while the bump broadens. Referring back to Fig. 2, these two ranges correspond to the exponential growth strongly increasing from  $d_i/d = 1.75$  to 2.5 but saturating for larger  $d_i/d$ . The increase of the growth rate with an increase in the density difference is expected for a RT instability [1, 2].

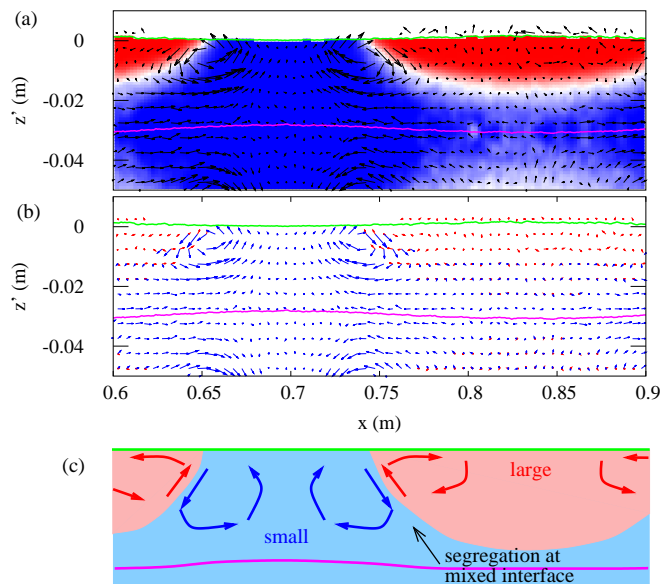


FIG. 5. Displacement vector maps (magnified 15 times) for (a) both species, and (b) each species multiplied by its volume fraction,  $f_i\phi$ , in the  $x - z'$  plane ( $y' = 0$ ) for fully developed axial segregation at  $t = 1300$  s. Colors in (a) correspond to  $f_l$  according to Fig. 3; red and blue vectors in (b) correspond to large and small particles, respectively. (c) Sketch of recirculation rolls in the large (red) and small (blue) particle regions. Green lines corresponds to the free surface and magenta lines to the lower limit of the free flowing layer.

**Recirculation rolls** — The usual ascending and descending plumes expected for both the granular and fluid RT instabilities that lead to an inversion of the two phases do not occur here. The descending plumes do not spread at the lower bound of the flowing layer but remain as fixed downward protrusions (Fig. 3(f)). The ascending plumes are not symmetric with the descending plumes. Ascending plumes may reach the free surface and form bands of pure small particles as observed here and in experiments or stay below the free surface in the case of subsurface bulges. Neither the ascending nor the descending plumes spread in the spanwise direction at the surface or at the bottom of the flowing layer as would occur in the fluid RT instability. Instead,

the combination of RT instability and segregation creates recirculation rolls in the  $x - z'$  plane (Fig. 5), shown as particle displacement vectors over a complete circuit through the flowing layer and solid body rotation based on the averaged velocity field. Figure 5(a) shows the vector displacement map for all particles overlaying the large particle volume fraction,  $f_l$ . There is a pair of relatively strong streamwise-oriented recirculation rolls on either side of the interface between the bands.

The ongoing vortical motion is decomposed into separate displacement vector maps for large and small particles in Fig. 5(b) based on their individual velocity fields, multiplied by the species volume fraction,  $f_i\phi$ . Areas with only one color of vectors have only one of the species present. The two species follow different paths: the small particle recirculation roll centered at  $x \approx 0.74$  m occurs in the mixed and small particle regions (Fig. 5(a)). The relative motion between the species is due to size segregation. As sketched in Fig. 5(c), the downward segregation of small particles at the mixed tilted region drives the small particle recirculation roll. At the same time a much weaker large particle recirculation roll (red) rotates in the same direction, driven by the upward segregation of the large particle in the tilted mixed region. The difference in the strength of the recirculation cells is likely due to the denser mixed region inducing a downward motion that favors the small particle recirculation rolls.

Here, the RT instability appears to initiate the formation of the bands and likely determines their wavelength, but the recirculation rolls are different from the Rayleigh-Bénard-like convection rolls for flow down an incline, where rolls extend through the entire flowing layer thickness with descending large-dense particle plumes and ascending plumes of mainly small-light particles flow [14]. Instead, there are twice as many rolls associated with axial bands in a tumbler, and they are in the upper part of the flowing layer, where the interface between the bands is tilted. The resulting large particle bands are also different in that they are wider and have an underlying core of mainly small particles. Furthermore, the downward

motion of descending plumes is controlled by the combined effects of diffusion, which favors mixing, and the subsequent increase in  $\phi$ , and segregation, which reduces mixing. As a plume sinks, its head reaches a region where  $\phi$  is higher and the velocity is lower, both enhancing segregation efficiency. The plume stops when a balance is obtained between the density excess, mixing, and segregation, thereby maintaining a frozen pattern of depth-wise protrusions and a stationary band pattern that can be visible at the surface

**Discussion**—These results explain how the granular RT instability initiates the formation of plumes leading to axial segregation. Simultaneously, pairs of segregation driven recirculation rolls develop on both sides of the tilted regions of the interface. This RT instability is unusual in the sense that that the third denser layer that appears between the large and small particle layers results from the mixture of granular species and does not have a constant volume. As a consequence, the final depth and shape of the bands result from a complex interaction between instability, mixing, and segregation. Axial bands form over a range rotation speeds, particle size ratios, tumbler diameters, fill levels, and particle densities, although the formation of bands is sensitive in varying degrees to these factors, all of which influence the RT instability, the segregation process, or both, and which will be explored extensively in a detailed companion paper. Even more intriguing are the questions of why the wavelength of the bands is approximately equal to the tumbler diameter, likely due to specific aspects of tumbler flow, and why the bands eventually coalesce to coarsen the band structure. The latter is likely a consequence of the complex interaction between the RT instability and particle segregation. Nevertheless, the current results finally resolve the long-standing question of the basic mechanisms behind the appearance of axially segregated bands for size-bidisperse iso-density species in a rotating tumbler that has long puzzled researchers.

**Acknowledgments**—This work was performed using HPC resources from GENCI-IDRIS (Grant 2022-102451).

- 
- [1] S. Chandrasekhar, *Hydrodynamic and Hydromagnetic Stability*, (Oxford University Press, London, 1961).
  - [2] F. Charru, *Hydrodynamic Instabilities*, (Cambridge University Press, Cambridge, 2011).
  - [3] M. R. Carey, S. W. Morris, and P. Kolodner, *Convective fingering of an autocatalytic reaction front*, Phys. Rev. E **53**, 6012 (1996).
  - [4] M. Böckmann and S. C. Müller, *Growth rates of the buoyancy-driven instability of an autocatalytic reaction front in a narrow cell*, Phys. Rev. Lett. **85**, 2506 (2000).
  - [5] J. Martin, N. Rakotomalala, D. Salin, and M. Böckmann, *Buoyancy-driven instability of an autocatalytic reaction front in a Hele-Shaw cell*, Phys. Rev. E **65**, 051605 (2002).
  - [6] C. Wylock, A. Rednikov, B. Haut, and P. Colinet, *Nonmonotonic Rayleigh-Taylor instabilities driven by gas-liquid CO<sub>2</sub> chemisorption*, J. Phys. Chem. B **118**, 11323 (2014).
  - [7] M. Abkarian, S. Protière, J. M. Aristoff, and H. A. Stone, *Gravity-induced encapsulation of liquids by destabilization of granular rafts*, Nat. Comm. **4**, 1895 (2013).
  - [8] S. Protière, C. Josserand, J. M. Aristoff, H. A. Stone, and M. Abkarian, *Sinking a granular raft*, Phys. Rev. Lett. **118**, 108001 (2017).
  - [9] N. Thomas, S. Tait, and T. Koyaguchi, *Mixing of stratified liquids by the motion of gas bubbles: application to magma mixing*, Earth Planet. Sci. Lett., **115**, 161 (1993).
  - [10] P. C. Matthews, *A model for the onset of penetrative convection*, J. Fluid Mech. **188**, 571 (1988).
  - [11] J. R. Lister and R. C. Kerr, *The effect of geometry on the gravitational instability of a buoyant region of viscous*

- fluid*, J. Fluid Mech. **202**, 577 (1989).
- [12] G. K. Batchelor and J. M. Nitsche, *Instability of stationary unbounded stratified fluid*, J. Fluid Mech. **227**, 357 (1991).
- [13] S. G. Yiantsios and B. G. Higgins, *Rayleigh–Taylor instability in thin viscous films*, Phys. Fluids A **1**, 1484 (1989).
- [14] U. D’Ortona and N. Thomas, *Self-induced Rayleigh–Taylor instability in segregating dry granular flows*, Phys. Rev. Lett. **124**, 178001 (2020).
- [15] M. B. Donald and B. Roseman, *Mixing and de-mixing of solid particles*, Br. Chem. Eng. **7**, 749 (1962).
- [16] G. H. Ristow, *Particle mass segregation in a two-dimensional rotating drum*, Europhys. Lett. **28**, 97 (1994).
- [17] E. Clément, J. Rajchenbach, and J. Duran, *Mixing of a granular material in a bidimensional rotating drum*, Europhys. Lett. **30**, 7 (1995).
- [18] J. Bridgewater, *Fundamental powder mixing mechanisms*, Powder Technol. **15**, 215–236 (1976).
- [19] K. M. Hill and J. Kakalios, *Reversible axial segregation of binary mixtures of granular materials*, Phys. Rev. E **49**, R3610 (1994).
- [20] K. Choo, M. W. Baker, T. C. A. Molteno and S. W. Morris, *Dynamics of granular segregation patterns in a long drum mixer*, Phys. Rev. E **58**, 6115 (1998).
- [21] A. Alexander, F. J. Muzzio, and T. Shinbrot, *Effects of scale and inertia on granular banding segregation*, Gran. Matter **5**, 171 (2004).
- [22] Y. Oyama, *Studies on mixing of solids. mixing of binary system of two sizes by ball mill motion*, Sci. Pap. Phys. Chem. Res. **37**, 17 (1940).
- [23] S. Das Gupta, D. V. Khakhar, and S. K. Bhatia, *Axial segregation of particles in a horizontal rotating cylinder*, Chem. Eng. Sci. **46**, 1513 (1991).
- [24] M. Nakagawa, *Axial segregation of granular flows in a horizontal rotating cylinder*, Chem. Eng. Sci. **49**, 2540 (1994).
- [25] O. Zik, D. Levine, S. G. Lipson, S. Shtrikman, and J. Stavans, *Rotationally induced segregation of granular materials*, Phys. Rev. Lett. **73**, 644 (1994).
- [26] K. M. Hill and J. Kakalios, *Reversible axial segregation of rotating granular media*, Phys. Rev. E **52**, 4393 (1995).
- [27] D. C. Rapaport, *Simulational studies of axial granular segregation in a rotating cylinder*, Phys. Rev. E **65**, 061306 (2002).
- [28] D. Levine, *Axial segregation of granular materials*, Chaos **9**, 573 (1999).
- [29] C. R. J. Charles, Z. S. Khan, and S. W. Morris, *Pattern scaling in axial segregation*, Gran. Matter **8**, 1 (2005).
- [30] S. J. Fiedor, P. Umbanhowar, and J. M. Ottino, *Pattern scaling in axial segregation*, Phys. Rev. E **73**, 041303 (2006).
- [31] G. Juarez, J. M. Ottino, and R. M. Lueptow, *Axial band scaling for bidisperse mixtures in granular tumblers*, Phys. Rev. E **78**, 031306 (2008).
- [32] G. Juarez, R. M. Lueptow, and J. M. Ottino, *Granular coarsening: Phase space and evolution analogies*, Phys. Rev. E **81**, 012301 (2010).
- [33] K. Choo, T. C. A. Molteno and S. W. Morris, *Traveling granular segregation patterns in a long drum mixer*, Phys. Rev. Lett. **79**, 2975 (1997).
- [34] V. Frette and J. Stavans, *Avalanche-mediated transport in a rotated granular mixture*, Phys. Rev. E **56**, 6981 (1997).
- [35] K. M. Hill, A. Caprihan, and J. Kakalios, *Axial segregation of granular media rotated in a drum mixer: Pattern evolution*, Phys. Rev. E **56**, 4386 (1997).
- [36] S. J. Fiedor and J. M. Ottino, *Dynamics of Axial Segregation and Coarsening of Dry Granular Materials and Slurries in Circular and Square Tubes*, Phys. Rev. Lett. **91**, 244301 (2003).
- [37] N. Jain, D. V. Khakhar, R. M. Lueptow, and J. M. Ottino, *Self-organization in granular slurries*, Phys. Rev. Lett. **86**, 3771 (2001).
- [38] T. Arndt, T. Siegmann-Hegerfeld, S. J. Fiedor, J. M. Ottino, and R. M. Lueptow, *Dynamics of granular band formation: Long-term behavior in slurries, parameter space, and tilted cylinders*, Phys. Rev. E **71**, 011306 (2005).
- [39] Z. S. Khan, W. A. Tokaruk, and S. W. Morris, *Oscillatory granular segregation in a long drum mixer*, Europhys. Lett. **66**, 212 (2004).
- [40] N. Taberlet, W. Losert, and P. Richard, *Understanding the dynamics of segregation bands of simulated granular material in a rotating drum*, Europhys. Lett. **68**, 522 (2004).
- [41] N. Taberlet, M. Newey, P. Richard, and W. Losert, *On axial segregation in a tumbler: an experimental and numerical study*, J. Stat. Mech. P07013 (2006).
- [42] P. Chen, J. M. Ottino, and R. M. Lueptow, *Granular axial band formation in rotating tumblers: a discrete element method study*, New J. Phys. **13**, 055021 (2011).
- [43] I. S. Aranson and L. S. Tsimring, *Dynamics of axial separation in long rotating drums*, Phys. Rev. Lett. **82**, 4643 (1999).
- [44] I. S. Aranson, L. S. Tsimring, and V. M. Vinokur, *Continuum theory of axial segregation in a long rotating drum*, Phys. Rev. E **60**, 1975 (1999).
- [45] T. Elperin and A. Vikhansky, *Mechanism of the onset of axial segregation in a rotating cylindrical drum filled with binary granular mixtures*, Phys. Rev. E **60**, 1946 (1999).
- [46] P. Chen, J. M. Ottino, and R. M. Lueptow, *Onset mechanism for granular axial band formation in rotating tumblers*, Phys. Rev. Lett. **104**, 188002 (2010).
- [47] D. C. Rapaport, *Radial and axial segregation of granular matter in a rotating cylinder: A simulation study*, Phys. Rev. E **75**, 031301 (2007).
- [48] N. A. Pohlman, J. M. Ottino, and R. M. Lueptow, *End-wall effects in granular tumblers: From quasi-two-dimensional flow to three-dimensional flow*, Phys. Rev. E **74**, 031305 (2006).
- [49] A. Santomaso, M. Olivi, and P. Canu, *Mechanisms of mixing of granular materials in drum mixers under rolling regime*, Chem. Eng. Sci. **59**, 3269 (2004).
- [50] P. Chen, J. M. Ottino, and R. M. Lueptow, *Subsurface granular flow in rotating tumblers: A detailed computational study*, Phys. Rev. E **78**, 021303 (2008).
- [51] U. D’Ortona, N. Thomas, and R. M. Lueptow, *Recirculation cells for granular flow in cylindrical rotating tumblers*, Phys. Rev. E **97**, 052904 (2018).
- [52] K. Kondo and H. Ebata and S. Inagaki, *Segregation patterns in rotating cylinders determined by the size difference, density ratio, and cylinder diameter*, Sci. Rep. **13**, 13495 (2023).
- [53] K. Lochmann, L. Oger, and D. Stoyan, *Statistical analysis of random sphere packings with variable radius distribution*, Solid State Sci. **8**, 1397 (2006).

- [54] D. Weaire and T. Aste, *The pursuit of perfect packing* (CRC Press, 2008).
- [55] P. A. Cundall and O. D. L. Strack, *A discrete numerical model for granular assemblies*, *Geotechnique* **29**, 47 (1979).
- [56] C. Kloss, C. Goniva, A. Hager, S. Amberger, and S. Pirker, *Models, algorithms and validation for opensource DEM and CFD-DEM*, *Prog. Comput. Fluid Dyn.* **12**, 140 (2012).
- [57] J. Schäfer, S. Dippel, and D. E. Wolf, *Force schemes in simulations of granular materials*, *J. Phys. I (France)* **6**, 5 (1996).
- [58] T. G. Drake and R. L. Shreve, *High-Speed Motion Pictures of Nearly Steady, Uniform, Two-Dimensional, Inertial Flows of Granular Material*, *J. Rheol.* **30**, 981 (1986).
- [59] S. F. Foerster, M. Y. Louge, H. Chang, and K. Allia, *Measurements of the collision properties of small spheres*, *Phys. Fluids* **6**, 1108 (1994).
- [60] C. P. Schlick, Y. Fan, A. B. Isner, P. B. Umbanhowar, J. M. Ottino, and R. M. Lueptow, *Modeling segregation of bidisperse granular materials using physical control parameters in the quasi-2D bounded heap*, *AIChE J.* **61**, 1524 (2015).
- [61] M. Larcher and J. T. Jenkins, *Segregation and mixing profiles in dense, inclined flows of two types of spheres*, *Phys. Fluids* **25**, 113301 (2013).
- [62] C. P. Schlick, A. B. Isner, P. B. Umbanhowar, J. M. Ottino, and R. M. Lueptow, *On mixing and segregation: From fluids and maps to granular solids and advection-diffusion systems*, *Ind. Eng. Chem. Res.* **54**, 10465 (2015).
- [63] J. M. N. T. Gray, *Particle segregation in dense granular flows*, *Annu. Rev. Fluid Mech.* **50**, 407 (2018).
- [64] A. M. Fry, P. B. Umbanhowar, J. M. Ottino, R. M. Lueptow, *Diffusion, mixing, and segregation in confined granular flows*, *AIChE J.* **65**, 875 (2019).